Self-Induced Roll Oscillations Measured on a Delta Wing/Canard Configuration

Joseph Katz*
San Diego State University, San Diego, California
and
Daniel Levin†
Technion R&D Foundation, Haifa, Israel

A small canard wing was installed in front of a delta wing mounted on a free-to-roll sting balance in a low-speed wind tunnel. The leading-edge vortices originating from the canard enhanced the self-induced roll oscillations at test conditions for which the basic delta wing would otherwise have been stable. Time-dependent roll angle and normal and side force data recorded during these oscillations are presented along with their phase relations. It was found that, with this combined canard/wing configuration, the range of the angle of attack at which self-induced oscillations occurred was extended up to an angle of attack of about 45 deg.

Nomenclature

AR_c = canard aspect ratio
AR_w = wing aspect ratio
b = wingspan
c = wing chord
C_ℓ = rolling moment coefficient = rolling moment/$\frac{1}{2}\rho V^2 S(b/2)$
C_N = normal force coefficient (in balance coordinates), = normal force/$\frac{1}{2}\rho V^2 S$
C_Y = side force coefficient (in balance coordinates), = side force/$\frac{1}{2}\rho V^2 S$
h = distance between canard's trailing edge and wing's apex
S = wing area
t = time
V = wind tunnel airspeed
α = angle of attack
ρ = air density
ϕ = roll angle
ϕ_{max} = amplitude of roll oscillations
ω = frequency of roll oscillations

Introduction

In recent years, the flight envelope and maneuverability of high-speed aircraft have been constantly increasing. Consequently, these aircraft frequently maneuver at high angles of attack, where flow separations and unsteady airloads are encountered. Because of these effects, some undesirable self-induced aircraft motions are often observed and, thus, require more detailed studies.[1,2] An experiment that sheds some light on this complex phenomenon was the investigation of the one-degree-of-freedom, subsonic, self-induced roll oscillation of slender delta wings. In these experiments,[3,4] as well as in the present experiment, the model was mounted on a sting balance in a free-to-roll manner. When the model's angle of attack was increased at a given airspeed V, a self-induced roll oscillation of the limit-cycle type would often develop, as is indicated by the arrow in Fig. 1. In situations where angle of attack was low enough (20 deg in Ref. 4) and the vortex pattern above the wing was symmetric, the oscillatory motion would not start. However, when a flow disturbance was introduced into the test section, the oscillations were initiated and sustained. The driving force for these oscillations, as most researchers agree,[3-9] is the dynamic vortex interaction and the associated flow lag effects caused by the motion of both the wing and the leading edge (LE) vortices. This flow lag affects both vortex strength and vortex position. This latter delay of the motion of the LE vortex, and its disposition compared to its steady-state location, is easy to detect by flow visualization. During the roll oscillations, the vortex system above the up-moving semiwing moves outboard (in the wing frame of reference) and closer to the surface[5,6] compared to the opposite semiwing. Consequently, a rolling moment in the direction of the rotation is generated near the wing leveled condition, thereby providing the energy to drive the motion.

In the present study, an experiment was carried out in order to show that wing rock phenomena can be induced, or its range can be extended, by introducing two strong vortices ahead of a main wing. This situation partially resembles the vortex structure of an aircraft having long strakes ahead of a swept wing. The approach used was to initiate the two strong LE vortices by mounting a small delta wing ahead of a main wing surface that otherwise would not undergo self-induced roll oscillations (at a given condition). If, as a result of the increased length and strength of the vortex cores, self-induced roll oscillations begin, it will provide further information about the geometric ratios between vortex length and wing span that cause self-induced oscillations. An additional objective of the present work was to improve the time-dependent data recording so that phase relations, within the measured quantities, could be resolved. Therefore, an improved digital data reduction system was used to analyze the recordings of the transmitted loads from the six component balance. The data reduction system was based on a VAX 780 computer, which allowed a much faster and more reliable data acquisition, compared with the analog system used for the experiments of Ref. 4. Furthermore, the friction in the bearings and in the roll-angle measuring potentiometer was reduced to expand the range of the expected oscillations.[5]

Wind Tunnel and Model Geometry

The geometry of the wing and canard model is shown in Fig. 2. The aspect ratio of the canard was 0.7 and of the wing exactly unity. This wing was the same one used for the ex-

Received May 19, 1985; presented as Paper 85-1830 at the AIAA 12th Atmospheric Flight Mechanics Conference, Snowmass, CO, Aug. 19-21, 1985; revision received Feb. 10, 1986.

*Professor, Department of Aerospace Engineering. Member AIAA.
†Head, Wind Tunnel Laboratory. Member AIAA.

periments reported in Ref. 4 (periodic oscillations could not be obtained then). The roller bearings and the potentiometer, which record the instantaneous roll angle, were modified in such a way that the friction was minimal (less than $0.2\ g \times cm$). The six-component measuring unit was located behind the two bearings and did not rotate with the model. Recorded forces (normal C_N and side force C_Y) were resolved in a balance-fixed coordinate system. The electrical signals, from the balance and potentiometer, were sent to the data reduction system and were digitally resolved. The error in the force data was less than $\pm 9\ g$, which is smaller than the vertical extent of the symbols that represent the data in the following figures. The lowest natural frequency of the wing balance unit was measured and found to be about 80 Hz. This value is much higher than the wing rock frequencies measured. The wing and the canard lay on the same plane and the distance h between them could be adjusted between 2 to 18 mm (Fig. 2). This parameter was later found to influence the results only marginally and therefore a clearance of $h=2$ mm was used throughout the reported data. The model was mounted on the sting balance (Figs. 1 and 2) such that its geometrical and rolling moment axes coincided with the balance axis. The cross section of the wind tunnel was 1×1 m and the model pitch axis was kept in the center of the test section as indicated in Fig. 1. The air velocity through the test section was 25 m/s, corresponding to a Reynolds number of 0.3×10^6, based on the wing's chord.

Results

The wind tunnel experiments consisted of static and dynamic tests (with and without the canard) and flow visualization. The static test results for the normal and side forces and for the rolling moment are presented in Fig. 3. These data were obtained with the "canard on" configuration, whereas the data for the "wing-only" configuration were reported in Ref. 4. The addition of the canard changed the static results by only a small amount because of its small surface area compared to the wing's area.

In the free-to-roll tests, the model was set at an angle of attack and then the oscillations were initiated either by the use of tunnel natural or by forced disturbances. In the free-to-roll tests of Ref. 4, the wing with $AR=1$ would not undergo self-induced roll oscillations, even when these oscillations were actively initiated. Installation of an improved potentiometer (to measure the roll angle) and improved bearings, reduced the rolling friction (to about $C_\ell = \pm 0.000034$) so that, eventually, a limit-cycle oscillation was obtained. The time history of this oscillation is given in Fig. 4. This difference in the aerodynamics of the wing (between the results of Ref. 4 and this experiment) indicates the influence of friction on the self-induced oscillations, as it was analyzed in Ref. 5. In the "wing-only" configuration, steady-state oscillations could be obtained with angles of attack of 25–39 deg. But since the basic vortex pattern above the wing is symmetrical in this range (at least up to 35 deg according to Ref. 10), the oscillations were usually not self-starting and an initial artificial disturbance had to be introduced to the flowfield.

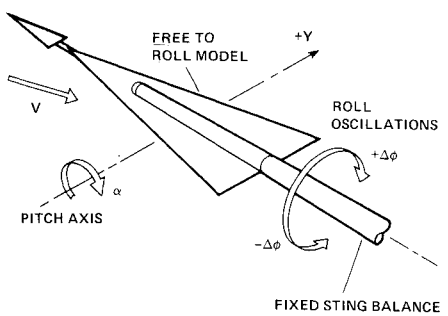

Fig. 1 Schematic description of the delta wing in the free-to-roll experiment.

The small canard was mounted ahead of the wing in order to initiate two strong upstream vortices. Because of the larger chordwise length of the combined canard/wing configuration, a longer time delay is expected between the wing's response and the changes in the location and strength of the LE vortices. Therefore, the addition of this canard can be viewed as an effective increase in the LE aft sweep that will bring the combined geometry into regions where self-induced oscillations have already been observed.[4] Consequently, it is expected that wing rock will take place at ranges of angle of attack where it was not possible with the "wing-only" configuration (at angles of attack of 19–44 deg).

The roll angle histories, at three different angles of attack, within the wing rock region, are presented in Fig. 5. The corresponding normal force and side force diagrams are presented in Figs. 6 and 7. When the range of both the normal and side force in the dynamic tests are compared with the static test values, a considerable loss in the vortex lift is detected. This loss in the normal force was shown in Ref. 4, but the present results with the canard show an even larger loss in this coefficient. The normal force oscillates (in Fig. 6) with two times larger frequency than the side force and the roll angle (Figs. 5 and 7). This was also reported in Refs. 3, 4, and 6 and was explained by the fact that the normal force does not change sign when the roll angle changes from right to left (positive to negative). Furthermore, the curves did not have a smooth sinusoidal shape, which is believed to be a result of the complex interaction among the four LE vortices originating from the wing and the canard.

In order to gain insight into the self-induced roll oscillation process, the C_ℓ vs ϕ histograms shown in Fig. 8 were plotted. The estimation of time-dependent rolling moment was obtained by computing the second derivative (with time) of the roll angle history (Fig. 5). This was done by fitting a cubic spline curve to the raw data of Fig. 5, with the maximal distance of any point from the spline curve being less than 1 deg, and then deriving numerically the second derivative. The results of these computations did depend on the order and on the maximal allowed deviations in the spline routine, but the typical shape of those curves was similar to those presented in Fig. 8 and in Ref. 3. A counterclockwise rotation of this diagram will mean that energy (integral of $C_\ell \cdot d\phi$) is dissipated by the damping force, while the clockwise rotation (found at the midrange) is an indication of energy being added to the system by the forces driving the oscillation. Thus, the aforementioned vortex interactions are generating the driving forces and moments for the oscillations near the $\phi=0$ (wing level) condition, as shown by Fig. 8. A comparison of the estimated rolling moments in Fig. 8 with the static data of Fig. 3 shows good agreement for $\alpha=20$ and 27 deg. For $\alpha=35$ deg, however, the static data are much smaller than the computed dynamic value, indicating that vortex breakdown in the dynamic case is delayed.

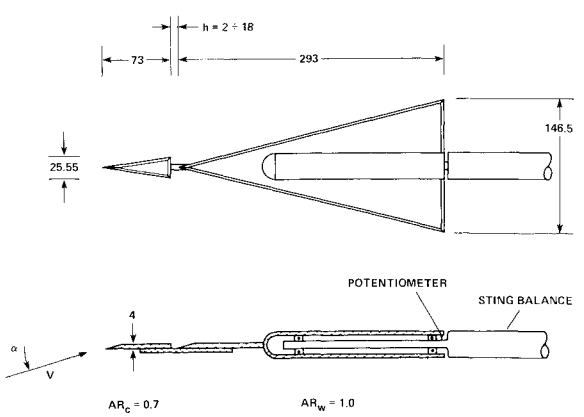

Fig. 2 Geometrical details of the model.

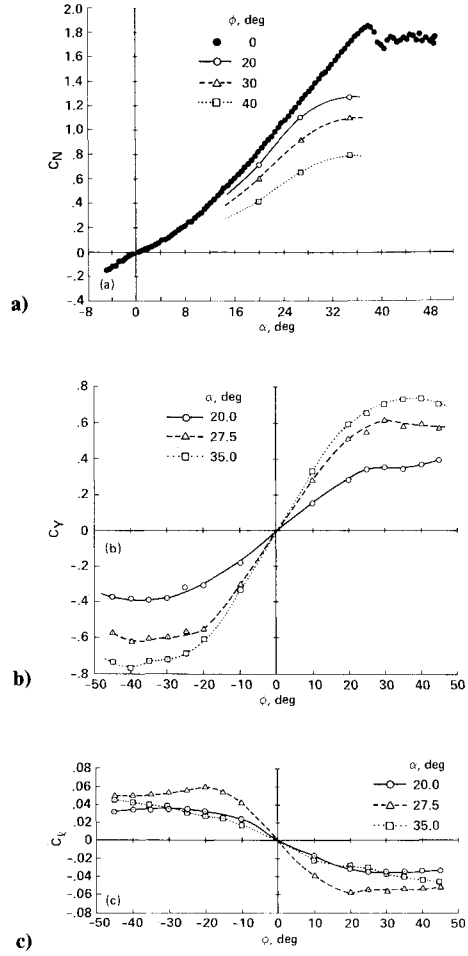

Fig. 3 Static data for a delta wing with $AR = 1$: a) normal force coefficient; b) side force coefficient; c) rolling moment coefficient.

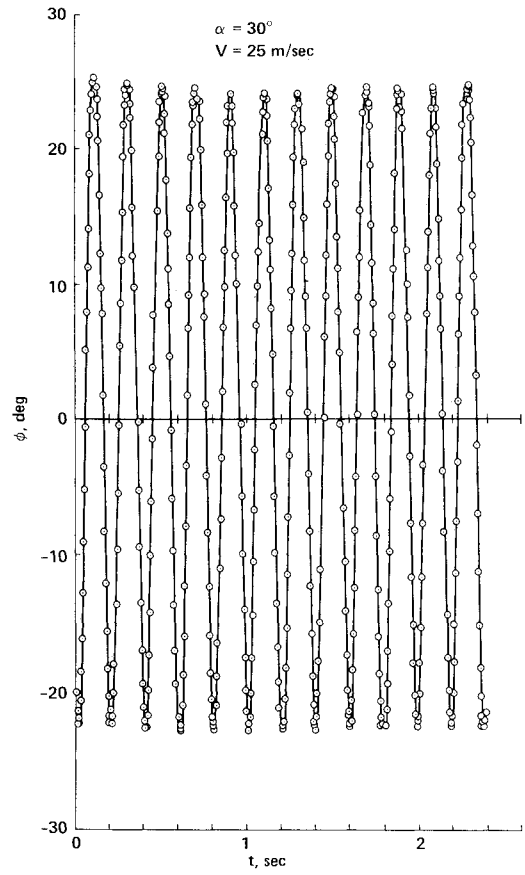

Fig. 4 Rolling angle time history (wing only).

The phase relations for the normal and side forces during the roll oscillations were plotted for $\alpha = 35$ deg in the histograms shown in Figs. 9 and 10, respectively. The drop in the normal force is again apparent and its magnitude is very high, even when it is compared with the value measured for "wing-only" configurations. Flow visualizations (by the helium/soap bubble technique) indicated that, during parts of the dynamic cycle, the canard vortices separate from the wing LE vortices and, therefore, the canard-induced vortex lift was reduced. This could result in an additional dislocation of the delta wing's LE vortices relative to their steady-state value and, consequently, even lower dynamic normal and side forces being measured.

The histogram of Fig. 9 shows the highly nonlinear dependence of the normal force on the roll angle. Basically, for the larger absolute roll angles, the normal force decreases because of the smaller, normal component of the onset flow, relative to the wing (Fig. 3). In the midrange of the diagram ($\phi \approx 0$ deg), a delay in the buildup of the normal force is visible. At the edges of the loop, a strong drop in the normal force (possibly due to vortex breakdown) is recorded, resulting in a damping effect that actually stabilizes the motion. The histogram of the side force (Fig. 10) exhibits similar behavior. The slope ($\partial C_Y/\partial\phi$) at the midrange is close to the steady-state value but, as a result of the reduced normal force, a noticeable loss in the side force is shown. At the loop edges (ϕ in the range of absolute 15 to 20 deg), again lower forces were measured due to vortex breakdown. However, at the midrange (e.g., for $\phi = 10$ deg), a higher side force was expected for the downward moving wing, corresponding to the results of the normal force. In this experiment, however, the wing had a central cylindrical body that was affected by the vortex being closer during the upward motion. Therefore, during the downward motion of the wing, a smaller side force was generated than during its motion to the opposite direction. The shape of these histograms remained similar to those presented in Figs. 9 and 10 for a large number of oscillatory cycles. On the other hand, a change in angle of attack did complicate their shapes and, at $\alpha = 27$ deg, two more loops were added (due to entanglement of the lines at $\phi = 0$). At $\alpha = 20$ deg, the loops became much smaller and the enclosed area was reduced beyond recognition, so that during some cycles a direction change in the rotation of the histogram was recorded.

Figure 11 summarizes the range of this experiment in terms of angle of attack and roll oscillation amplitudes. The "wing-only" configuration oscillated at the shown range of $\alpha = 25$–39 deg. The canard-induced oscillations, however, covered a much wider range of angles of attack. This oscillation started at about 19 deg and roll amplitude increased rapidly up to $\alpha = 30$ deg. Flow visualization (a schematic description of which is inserted in Fig. 11) indicated that, at this range of angle of attack, the canard and the wing LE vortices combined into one concentrated vortex throughout most of the oscillation cycle. At about $\alpha = 30$ deg, the fore-and-aft oscillatory motion of the vortex breakdown had reached the wing trailing edge and the damping effect had started to reduce the roll angle amplitude. At about $\alpha = 44$ deg, the breakdown of the canard vortices reached the canard's trailing edge, while on the wing the breakdown pattern moved ahead of the trailing edge. The damping effect of this vortex breakdown resulted in the cessation of the oscillatory rolling motion. Further increase in the angle of attack of the model resulted in a nonsymmetric vortex pattern and the model stabilized at $\phi \neq 0$ accompanied by random, damped, small-amplitude oscillations (as shown in Fig. 11 for the range of $\alpha = 47$–51 deg). Moving

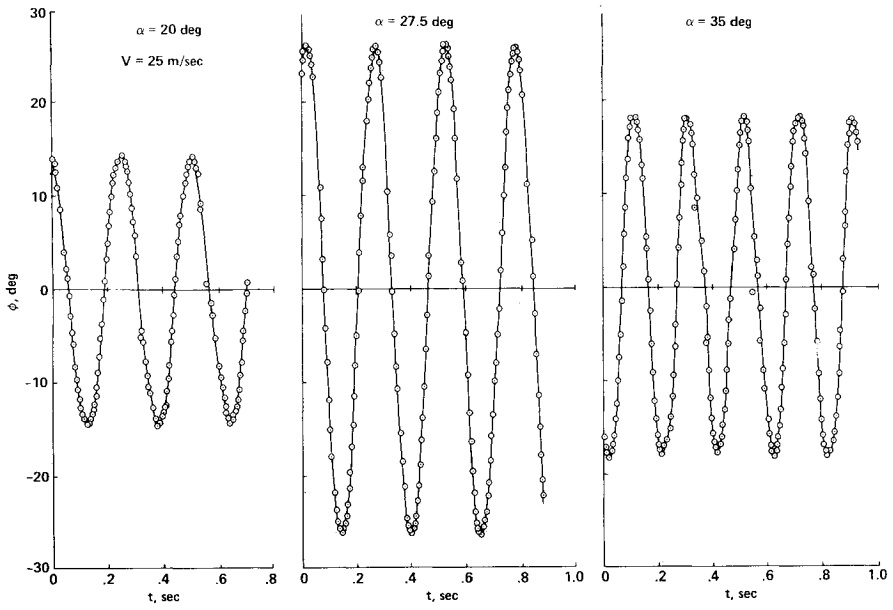

Fig. 5 Rolling angle time history (wing and canard).

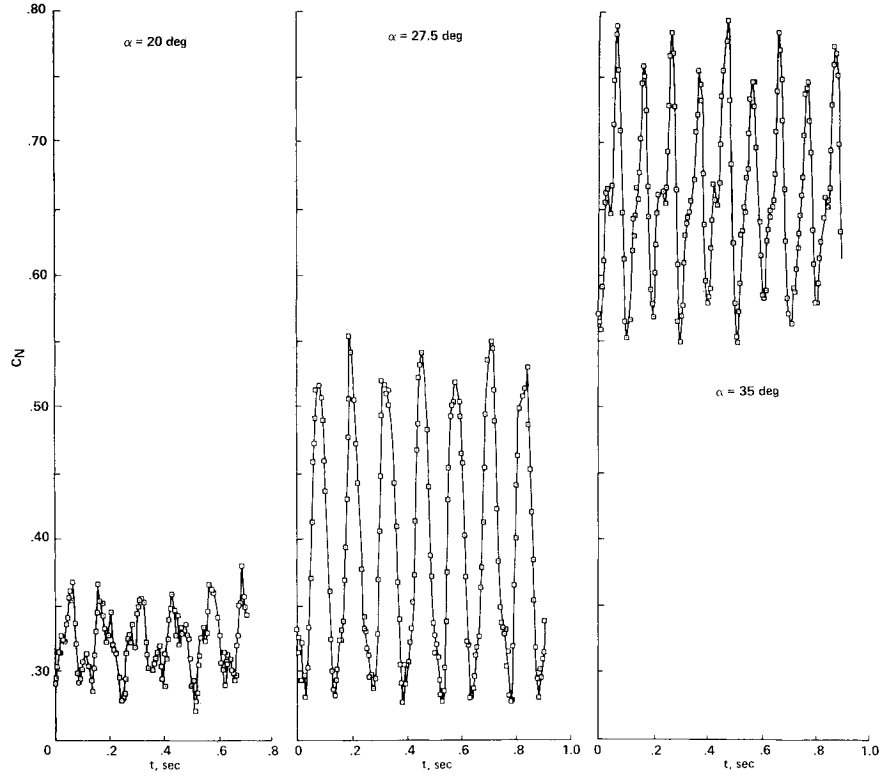

Fig. 6 Time history of the normal force in a free-to-roll test.

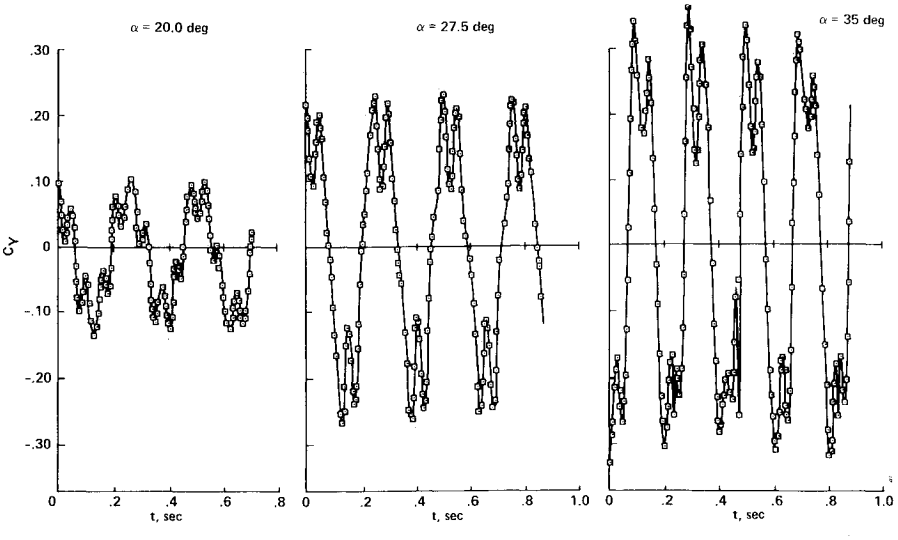

Fig. 7 Time history of the side force in a free-to-roll test.

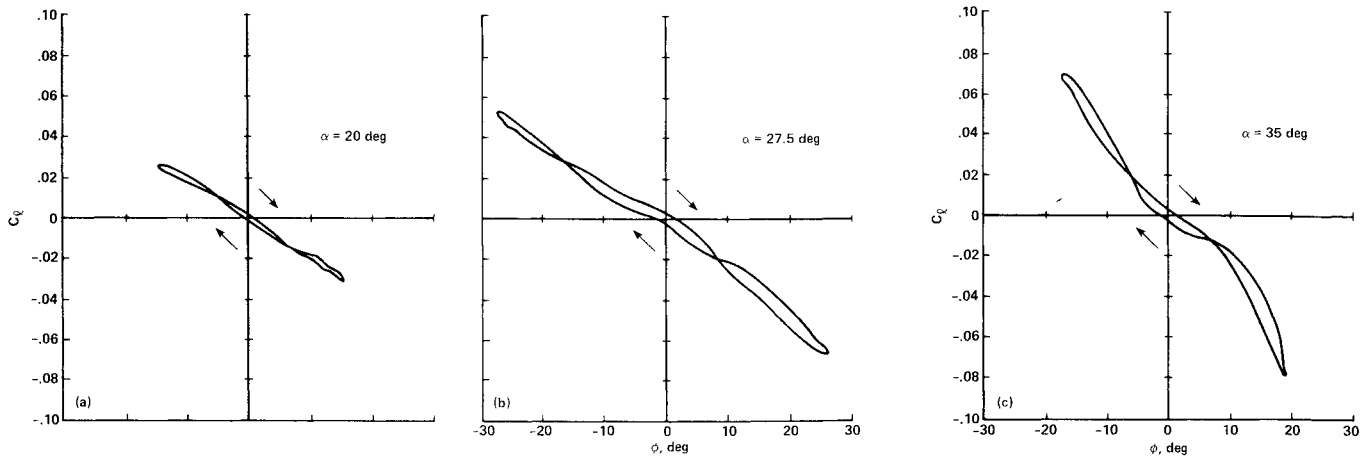

Fig. 8 Histogram of the rolling moment during a wing rock cycle.

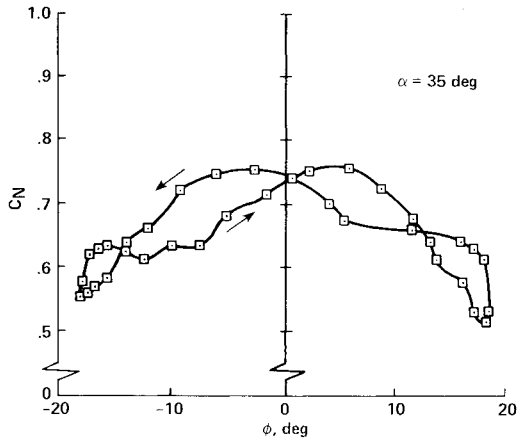

Fig. 9 Histogram of the normal force coefficient during a wing rock cycle.

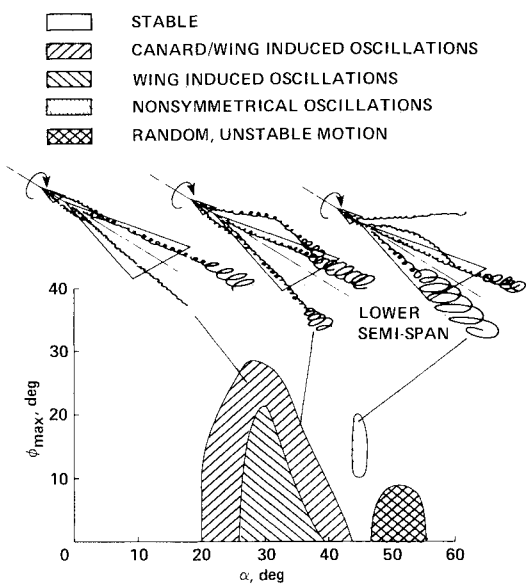

Fig. 11 Region of self-induced roll oscillations for the current experiment.

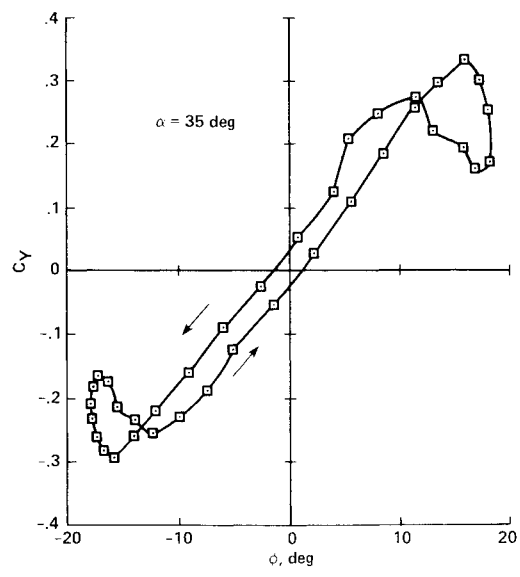

Fig. 10 Histogram of the side force coefficient during a wing rock cycle.

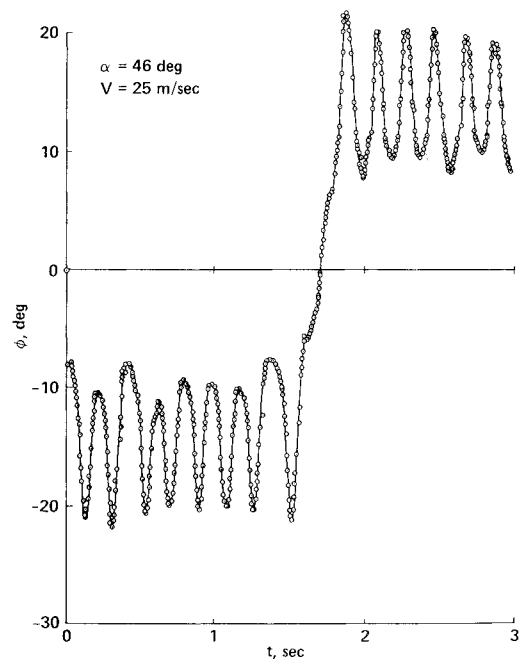

Fig. 12 Rolling angle time history for asymmetric oscillation.

the canard to its maximum forward position of $h = 18$ mm, as indicated in Fig. 2, slightly increased roll angle amplitude at $\alpha = 19$ deg. Beyond $\alpha = 23$ deg, the roll amplitude was less by about 3-5 deg (compared to Fig. 11) and the oscillations ceased earlier ($\alpha = 42$ deg). Further investigation of this parameter was not done in this investigation, but it is expected that for larger values of h the canard/wing vortex interaction will become insignificant.

At the range of $\alpha = 44$–46 deg, antisymmetric oscillations were observed at about $\phi = \pm 15$ deg and a recording of the roll angle history is given in Fig. 12. At this condition, one of the canard's LE vortices was captured by the higher, opposite semiwing (see insert in Fig. 11), while its other LE vortex was directly shed into the flow. Also, at the lower semispan of the wing, a major vortex breakdown pattern was visible. Any small disturbance in the flowfield could flip the wing from positive to negative roll amplitudes (and vise versa). After an elaborative recording of the data (showing the transition), Fig. 12 was obtained.

Conclusions

The results of this experiment reinforce the hypothesis that the subsonic wing rock phenomenon of slender wings is caused by dynamic vortex interaction with the lifting surface. By adding the canard, the effective aspect ratio of the configuration was reduced to ranges where self-induced oscillations were observed before. Consequently, the range of the wing rock for the delta wing with an aspect-ratio of one was enlarged. It has also been shown that vortex interactions can result in very complex and not easily predictable flowfield conditions. The nonsymmetric oscillations obtained in this test are a good example of how the presence of four concentrated vortices, instead of two in the case of a single delta wing, did complicate the motion.

Acknowledgments

The authors appreciatively acknowledge the support provided by the Aeronautical Research Center at Technion—Israel Institute of Technology.

This work was done while the first author held a NRC Senior Research Associateship at NASA Ames Research Center.

References

[1]Orlic-Rukemann, K.J., "Aerodynamic Aspects of Aircraft Dynamics at High Angles of Attack," *Journal of Aircraft*, Vol. 20, Sept. 1983, pp. 737–752.

[2]Schmidt, L.V., "Wing Rock Due to Aerodynamic Hysteresis," *Journal of Aircraft*, Vol. 16, March 1979, pp. 129–133.

[3]Nguyen, L.T., Yip, L., and Chambers, J.R., "Self Induced Wing Rock of Slender Delta Wings," AIAA Paper 81-1883, Aug. 1981.

[4]Levin, D. and Katz, J., "Dynamic Load Measurements with Delta Wings Undergoing Self-Induced Roll Oscillations," *Journal of Aircraft*, Vol. 21, Jan. 1984, pp. 30–36.

[5]Konstadinopoulos, P., Mook, D.T., and Nayfeh, A.H., "Numerical Simulation of the Subsonic Wing Rock Phenomenon," AIAA Paper 83-2115, Aug. 1983.

[6]Ericsson, L.E., "The Fluid Mechanics of Slender Wing Rock," *Journal of Aircraft*, Vol. 21, May 1984, pp. 322–328.

[7]Ericsson, L.E., "Flow Phenomena Causing Wing and Body Rock," AIAA Paper 84-2177, Aug. 1984.

[8]Konstadinopoulos, P., Mook, D.T., and Nayfeh, .H., "Subsonic Wing Rock of Slender Delta Wings," *Journal of Aircraft*, Vol. 22, Oct. 1985, pp. 920–924.

[9]Hsu, C.H. and Lan, C.E., "Theory of Wing Rock," AIAA Paper 85-0199, Jan. 1985.

[10]Polhamus, E.C., "Predictions for Vortex Lift Characteristics by Leading Edge Suction Analogy," *Journal of Aircraft*, Vol. 8, April 1971, pp. 193–199.